Magnetic Susceptibility Estimation for Magnetostatics

Vijn, Aad; Lepelaars, Eugene; Dubbeldam, Johan; Van Gijzen, Martin; Heemink, Arnold

DOI
10.1109/TMAG.2019.2892346

Publication date
2019

Document Version
Final published version

Published in
IEEE Transactions on Magnetics

Magnetic Susceptibility Estimation for Magnetostatics

Aad Vijn[1], Eugene Lepelaars[2], Johan Dubbeldam[1], Martin van Gijzen[1], and Arnold Heemink[1]

[1]Delft Institute of Applied Mathematics, Delft University of Technology, 2600 AA Delft, The Netherlands
[2]Electronic Defence, Netherlands Organisation for Applied Scientific Research, 2509 JG The Hague, The Netherlands

This paper presents a parameter estimation method to determine the linear behavior of an object constructed of thin plates. Based on the magnetostatic field equations, an integral equation is derived that fully determines the induced magnetization, whenever the spatial magnetic susceptibility distribution is known. This forward problem is used as an underlying physical model for the parameter estimation method. Using near-field magnetic measurements around a thin plate, the parameter estimation yields a distribution of the magnetic susceptibility. Furthermore, a sensitivity analysis is performed to understand the behavior of this parameter estimation method.

Index Terms— **Forward problem, induced magnetization, inversion, magnetic susceptibility, parameter estimation, regularization.**

I. Introduction

IDENTIFICATION of the magnetic state of ferromagnetic objects is, in general, very difficult. A common approach is to split the total magnetization into two parts: an induced part and a permanent part. The induced magnetization is related to a linear response of the material to the background field, and the permanent part is due to the magnetic history of the material [16]. The magnetic history, also called magnetic hysteresis, is a very complex phenomenon that may be described by means of Preisach models [18] or continuous models such as Jiles and Atherton [11]. The linear response is described by the magnetic susceptibility and may be complex to describe depending on the material properties. Isotropic material does not have a preferred direction in which it magnetizes, and therefore, the magnetic susceptibility is easily described by a scalar quantity. For anisotropic materials, the magnetic susceptibility is harder to describe because of the orientation dependencies within the material.

A related notion to the magnetic susceptibility is the (relative) permeability, which seems to be more relevant in applications. The magnetic susceptibility χ and relative permeability μ_r are related to the well-known identity

$$\chi + 1 = \mu_r.$$

Hence, all results in this paper (in terms of the magnetic susceptibility) can equivalently be expressed in terms of the permeability. From our point of view, we are interested in the magnetic susceptibility, because it links the internal magnetic field inside an object to its magnetization.

A typical application of identifications of magnetic states can be found in the military context. Nowadays, accurate identification of the magnetic state of a military vessel (called the magnetic signature) has become important, as more sophisticated weaponry use different kinds of sensors—such as magnetic sensors—to find and destroy their target. It is of utmost importance for the navy to reduce the magnetic signature of their military vessels, to avoid detection and destruction of their vessels [7]–[9].

The forward computation of the induced magnetization is rather simple and can be done in a finite-element environment. Such implementations are readily available in many software packages such as `Comsol Multiphysics`, `Cédrat Flux3D`, and `Ansys Maxwell`. However, for such computations of the induced magnetization, the value of the magnetic susceptibility χ must be known. In the literature, one can find specific values for different materials. In practice, anomalies in materials and the specific composition of the material imply variations in these values. Therefore, one should expect spatial variability of χ in an object rather than being a constant. This makes accurate modeling of the forward problem complicated.

Several parameter estimation methods have been proposed for the determination of the magnetic susceptibility. Susceptibility estimation is found in the determination of the initial magnetic susceptibility for the "metal magnetic memory" method to passive magnetic nondestructive testing [17]. Even though MRI works with a high-frequency signal, a magnetic susceptibility method can be defined in magnetostatics by considering the relationship between the magnetic susceptibility and varying magnetic fields in the frequency domain (for a fixed frequency) [12]. However, for MRI-related applications, the values of the magnetic susceptibility are presumed to be small (in the order of 10^{-3}), which leads to approximately linear estimation models. For ferromagnetic steel, the magnetic susceptibility values are high (in the range of 10^2–10^5), which leads to nonlinear magnetic field equations in χ. This case is more challenging, and the techniques used are more involved.

This paper considers two topics. First, we derive a magnetic susceptibility estimation method to compute spatial magnetic susceptibility distributions of linearly reacting materials, for which the magnetic susceptibility values are large. This method is based on least-squares optimization and solved using the "Broyden–Fletcher–Goldfarb–Shanno (BFGS)" method [13]. Because approximations of these spa-

Manuscript received January 28, 2018; revised April 19, 2018; accepted December 28, 2018. Date of publication January 31, 2019; date of current version February 15, 2019. Corresponding author: A. Vijn (e-mail: a.r.p.j.vijn@tudelft.nl).

Color versions of one or more of the figures in this paper are available online at http://ieeexplore.ieee.org.

Digital Object Identifier 10.1109/TMAG.2019.2892346

tial magnetic susceptibility distributions may contain errors, we are interested in how these variations relate to the corresponding variations in the induced magnetic induction field. Such insights may also tell us to what extent the parameter estimations must be accurate. It is also important for future work, where we try to describe the magnetic distortion fields of magnetic objects accurately. These sensitivity questions are considered in the second part of this paper.

This paper has the following structure. In Section II, the methodology behind the derived magnetic susceptibility estimation is discussed. A forward model is derived that fully describes the linear behavior. Several magnetic identification methods are proposed for semi-linearly reacting materials [3], [4], [19]. However, we take another, slightly different, approach to describe the induced magnetization. From a physical point of view, we assume that magnetization is a continuous vector field. Therefore, we expand any magnetization as a function in terms of linear basis functions. This has some advantages, e.g., enabling the use of smoothing regularization operators. Then, using various techniques from variational data assimilation [5], [20] and numerical analysis [6], we solve the proposed nonlinear minimization problem. In Section III, numerical examples are given that illustrate the forward and magnetic susceptibility estimation. A numerical identical-twin experiment where the true magnetic susceptibility state is assumed to be known is conducted to test the validity of the methodology. In this stage of the research, it is essential to consider first a numerical validation of the method, because the true magnetic susceptibility state of magnetic objects is unknown in practice, and therefore, the performance of the method is hard to analyse. In Section IV, a sensitivity analysis is then performed to investigate the behavior of variations in the magnetic susceptibility in forward computations. A conclusion and a discussion of future work for the further enhancement of the proposed parameter estimation method are summarized in Section V.

II. Methodology

In this section, the methodology behind the parameter estimation method is discussed. Starting with the derivation of the underlying physical model, the parameter estimation method is then derived using techniques from variational data assimilation.

A. Magnetostatics

Suppose that an object is made of linearly reacting and isotropic material, and suppose that the magnetic susceptibility χ and the geometry of the object are known. Furthermore, assume that the object is made of thin plates with a thickness t.

The object is placed in a uniform magnetic background field $\mathbf{B}_0 = \mu_0 \mathbf{H}_0$. The background field induces some magnetization denoted by $\mathbf{M}^{\text{ind}}$. Assume that any permanent magnetization is absent, therefore, the magnetization of Ω reads

$$\mathbf{M} := \mathbf{M}^{\text{ind}}.$$

Due to the induced magnetization, a perturbation arises and this perturbation is called the reduced (or induced) magnetic field, denoted by $\mathbf{H}_{\text{red}}$. The total field $\mathbf{H}$ reads

$$\mathbf{H} = \mathbf{H}_0 + \mathbf{H}_{\text{red}}. \tag{1}$$

Let $\Omega \subseteq \mathbb{R}^3$ be the compact volume of the object. The linear behavior in Ω is defined through

$$\mathbf{M} = \chi \mathbf{H} \tag{2}$$

which defines the coupling between the magnetic field and the magnetization of object Ω. Here, χ is a dimensionless number, which is assumed to be spatially dependent.

To obtain the reduced magnetic field due to $\mathbf{M}$, use the magnetostatic field equations

$$\begin{cases} \nabla \times \mathbf{H} = \mathbf{0} \\ \nabla \cdot \mathbf{B} = 0 \\ \mathbf{B} = \mu_0(\mathbf{H} + \mathbf{M}). \end{cases} \tag{3}$$

In these equations, $\mathbf{B}$ denotes the magnetic induction field, and $\mu_0 = 4\pi \cdot 10^{-7}$ H/m is the magnetic permeability in vacuum. The magnetostatic equations can be solved via a scalar potential function (see [10, pp. 194–197]). The reduced magnetic field at point $\mathbf{r}$ reads

$$\mathbf{H}_{\text{red}}(\mathbf{r}) = -\frac{1}{4\pi} \iiint_{\Omega} \frac{\mathbf{r}-\mathbf{r}'}{|\mathbf{r}-\mathbf{r}'|^3} (\nabla' \cdot \mathbf{M})(\mathbf{r}') d\Omega' + \frac{1}{4\pi} \iint_{\partial\Omega} \frac{\mathbf{r}-\mathbf{r}'}{|\mathbf{r}-\mathbf{r}'|^3} (\mathbf{n}' \cdot \mathbf{M})(\mathbf{r}') dS' \tag{4}$$

where $\mathbf{n}' = \mathbf{n}'(\mathbf{r}')$ is a normal vector, pointing outwards. The differential operator ∇' is defined by $\nabla' = [\partial_{x'}, \partial_{y'}, \partial_{z'}]^T$. The magnetization $\mathbf{M}$ is supported on Ω, and $\mathbf{M} \equiv \mathbf{0}$ outside Ω.

Combining (1), (2), and (4) leads to the following integral equation for $\mathbf{M}$ (see [19])

$$\frac{1}{\chi(\mathbf{r})} \mathbf{M}(\mathbf{r}) + \frac{1}{4\pi} \iiint_{\Omega} \frac{\mathbf{r}-\mathbf{r}'}{|\mathbf{r}-\mathbf{r}'|^3} (\nabla' \cdot \mathbf{M})(\mathbf{r}') d\Omega' - \frac{1}{4\pi} \iint_{\partial\Omega} \frac{\mathbf{r}-\mathbf{r}'}{|\mathbf{r}-\mathbf{r}'|^3} (\mathbf{n}' \cdot \mathbf{M})(\mathbf{r}') dS' = \mathbf{H}_0. \tag{5}$$

Note that this equation is only valid *inside* the object Ω. Evaluation of (5) in a point $\mathbf{r} \in \Omega$ is mathematically challenging, since both integrals are singular for $\mathbf{r}' = \mathbf{r}$. Equation (5) must be reformulated in such a way that these singularities are avoided. This is done after discretization of Ω, using Gauss' divergence theorem.

B. Discrete Forward Problem

Introduce a triangulation of $\Omega = \bigcup_{k=1}^{N_e} e_k$ where N_e is the number of triangular elements. Because Ω is thin, we assume in the remainder of this paper that Ω is a 2-D surface and that the elements e are flat triangles. Using demagnetization factors [14], one can derive that, in this case, the magnetization is approximately tangential to the object and as χ is large, the induced magnetization is approximately uniform in the normal direction. In Fig. 1, one can find an example of a triangulation of a square plate. Furthermore, assume that χ is piecewise constant on each triangular element

$$\chi = \chi_k \text{ on element } e_k, \quad \chi_k \in \mathbb{R}_0^+. \tag{6}$$

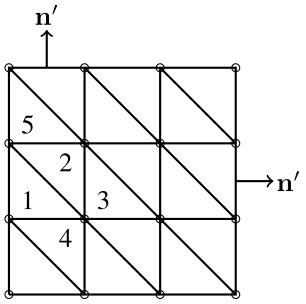

Fig. 1. Example of a triangulation, with triangular elements $e_1, \ldots, e_5$.

The next step is to approximate the magnetization $\mathbf{M}$ on each element. We choose to expand $\mathbf{M}$ in terms of linear basis functions. On a triangular element e, the approximation of $\mathbf{M}$ is denoted by $(\mathbf{M})_e$ and reads

$$(\mathbf{M})_e(\mathbf{r}) = \sum_{k=1}^{3} \mathbf{M}_k \varphi_k(\mathbf{r}) \tag{7}$$

where $\mathbf{M}_k$ are the values of $\mathbf{M}$ at the vertices $\mathbf{v}_1, \mathbf{v}_2$, and $\mathbf{v}_3$ of the triangular element e and φ_1, φ_2, and φ_3 are linear basis functions on e defined by the relations

$$\varphi_i(\mathbf{v}_j) = \delta_{ij}, \quad \text{for } i, j = 1, 2, 3. \tag{8}$$

The divergence of $\mathbf{M}$ and the flux $\mathbf{n}' \cdot \mathbf{M}$ is approximated using these expansions

$$(\nabla' \cdot \mathbf{M})_e(\mathbf{r}') = \sum_{k=1}^{3} \mathbf{M}_k \cdot \nabla' \varphi_k(\mathbf{r}') \tag{9}$$

and

$$(\mathbf{n}' \cdot \mathbf{M})_e(\mathbf{r}') = \sum_{k=1}^{3} (\mathbf{n}' \cdot \mathbf{M}_k) \varphi_k(\mathbf{r}'). \tag{10}$$

Using the triangulation and the above-mentioned expansions for $\mathbf{M}$, integral equation (5) is reduced to a finite-dimensional system of equations. Due to the small thickness of Ω, the volume and surface integrals in (5) are reduced to surface and line integrals. After applying a Galerkin projection method,[1,2] one obtains the following set of equations:

$$\frac{1}{\chi(\mathbf{r}_i)} (\mathbf{M})_{e_k}(\mathbf{r}_i) + \frac{t}{4\pi} \sum_e \int_{\partial e} \frac{\mathbf{n}'}{|\mathbf{r}_i - \mathbf{r}'|} (\nabla' \cdot \mathbf{M})_e(\mathbf{r}') dS' - \frac{t}{4\pi} \sum_e \int_{\partial \Omega \cap e} \frac{\mathbf{r}_i - \mathbf{r}'}{|\mathbf{r}_i - \mathbf{r}'|^3} (\mathbf{n}' \cdot \mathbf{M})_e(\mathbf{r}') dl' = \mathbf{H}_0 \tag{11}$$

for each evaluation point $\mathbf{r}_i \in e_k$. The normal vector $\mathbf{n}'$ is defined as a vector pointing outwards as illustrated in Fig. 1. Each evaluation of (11) in a point leads to a single equations in terms of the background field $\mathbf{H}_0$, the magnetic susceptibility values and magnetization values $\mathbf{M}_k$ at the grid points.

If the integral equation is evaluated in three points per triangular element e_k, the above-mentioned integral equation (5) can be solved consistently by solving the corresponding discrete system (11). Further derivations show that (11) can be written as a system of the form

$$\left[\sum_{k=1}^{N_e} \frac{1}{\chi_k} D_k + A + B \right] \mathbf{M} = \mathbf{h}_0. \tag{12}$$

The matrices $D_k, A, B \in \mathbb{R}^{3M \times 3N}$, where M is the number of evaluation points and N is the number of grid points and $\mathbf{h}_0 \in \mathbb{R}^{3M}$ is a constant vector that contains the magnetic background field. Vector $\mathbf{M} \in \mathbb{R}^{3N}$ is now the numerical approximation of the magnetization and contains the values of the magnetization in each of the grid points. Note that this vector suffices to describe the full magnetization through (7). Furthermore, the entries of D_k, A, and B may be computed analytically, or approximated numerically by means of suitable quadrature rules.

Finally, if $\mathbf{M}$ is obtained after solving (12), the same triangulation and expansion are used to compute the (total) magnetic induction field at any observation point via

$$\mathbf{B}^c(\mathbf{r}_k) = \mathbf{B}_0 + \mathbf{B}_{\text{red}}(\mathbf{r}_k) \tag{13}$$

where $\mathbf{B}_{\text{red}}(\mathbf{r}_k)$ is written as

$$\mathbf{B}_{\text{red}}(\mathbf{r}_k) = \mu_0 C(\mathbf{r}_k) \mathbf{M}. \tag{14}$$

The matrix $C(\mathbf{r}_k) \in \mathbb{R}^{3 \times 3N}$ is obtained from (4) after applying the discretization and evaluation at $\mathbf{r}_k$.

C. Inverse Problem Formulation

Based on the discrete forward problem described in Section II-B, one can formulate the corresponding (discrete) inverse problem. Suppose that the magnetic induction field of some linearly reacting magnetic object Ω is measured, the inverse problem is to determine the magnetic source $\mathbf{M}^{\text{ind}}$, based on the physical model described in Section II-B.

If $\mathcal{M} = \{\mathbf{r}_1, \mathbf{r}_2, \ldots, \mathbf{r}_K\}$ denotes a collection of measurement locations, the values of the magnetic induction field in the measurement locations give rise to a vector $\mathbf{B}^m \in \mathbb{R}^{3K}$ given by

$$\mathbf{B}^m = [(\mathbf{B}^m(\mathbf{r}_1))_x, (\mathbf{B}^m(\mathbf{r}_1))_y, (\mathbf{B}^m(\mathbf{r}_1))_z, \ldots (\mathbf{B}^m(\mathbf{r}_K))_x, (\mathbf{B}^m(\mathbf{r}_K))y, (\mathbf{B}^m(\mathbf{r}_K))_z]^T. \tag{15}$$

Each measurement is contaminated by noise; in this paper, we assume the Gaussian white noise and write

$$\mathbf{B}^m := \mathbf{b}_0 + \mathbf{B}^e_{\text{red}} + \mathbf{e}, \quad \mathbf{e} \sim \mathcal{N}(0, \Sigma) \tag{16}$$

where Σ is the covariance matrix of $\mathbf{e}$, $\mathbf{B}^e_{\text{red}}$ are the exact values of the reduced magnetic induction field, and $\mathbf{b}_0 \in \mathbb{R}^{3K}$ is a constant vector containing the values of the magnetic background induction field. Similarly, using the discrete forward model, one can compute the magnetic induction field in the measurement locations for some prescribed magnetic

[1] A word of caution on the reduction of the integral equation to the discrete case. Whenever the diameter of the triangular elements e_k becomes smaller than the thickness t of object Ω, then approximation (11) of integral equation (5) becomes invalid.

[2] In the derivation of (11), the assumptions are used in a slightly different order. One first start with a discretization of the full 3-D object Ω, and uses the typical value of the thickness to neglect terms of the equation. One is then left with integrals defined on the surface of the 3-D object, as mentioned in (11).

susceptibility distribution. This forward computation gives rise to a vector $\mathbf{B}^c[\chi]$ that is computed via a simple matrix product

$$\mathbf{B}^c[\chi] := \mathbf{b}_0 + C(\mathcal{M})\mathbf{M} \tag{17}$$

where $C(\mathcal{M}) \in \mathbb{R}^{3K\times 3N}$ is built out of block matrices defined in (14).

D. Inversion, Minimization Problem

System (12) and expressions (15) and (17) are the starting point of the derivation of the parameter estimation method. The idea is as follows: based on near-field measurements of the magnetic field $\mathbf{B}$, the task is to find a suitable spatial distribution of χ such that there is a good fit between computed values and the measured values. This naturally results in defining the residual

$$\mathbf{Res} := \mathbf{B}^m - \mathbf{B}^c[\chi]. \tag{18}$$

If the residual is small, a good fit between the measured values and computed values is expected, and the choice of the corresponding spatial distribution of χ should be acceptable. Define the residual functional

$$\mathcal{J}(\chi) = \frac{1}{2}\mathbf{Res}^T W \mathbf{Res} = \frac{1}{2}\|\mathbf{Res}\|_W^2 \tag{19}$$

where $W = \Sigma^{-1}$ is the inverse of the covariance matrix. Note that $\mathcal{J}$ depends on χ, although this dependence is not explicitly visible from its definition. The parameter estimation method is based on the iterative minimization of this functional. A solution of the parameter estimation method is found through

$$\chi^* = \underset{\chi\in\mathbb{R}^{N_e}}{\operatorname{argmin}}\, \mathcal{J}(\chi). \tag{20}$$

In practice, measurements are contaminated by noise. Noise typically arises from measurement interference and inaccuracies in the measuring devices; for magnetic field sensors, these inaccuracies are, e.g., orthogonality errors between axes, temperature dependencies, hysteresis in the device and scaling errors. This implies that whenever one tends to solve (20), a certain tolerance level ε_{tol} should be chosen in such a way that it reflects the noise level in the measurements (16)

$$\texttt{stop whenever } |\mathcal{J}(\chi^*)| < \varepsilon_{\text{tol}}. \tag{21}$$

Otherwise, the minimization will overfit the noise in the measurements, which leads to unsatisfying solutions.

E. Inversion, Regularization

In general, the solution of least-squares problem (20) is not unique, and $\mathcal{J}(\chi)$ has many local minima. In order to choose the optimal minimizer, additional information can be added to the least-squares problem to reduce the dimensions of the solution space.

In the literature, the values of χ for different materials can be found. This information can be used as a prior estimation of the χ-distribution in the minimization to guide the search of the solution, denoted by χ_{prior}.

In addition, one may require that χ satisfies a smoothness condition [2, Ch. 3.2]. Such a condition can be formalized in terms of a smoothing operator, say R, which originates from application of finite differences to χ. Smoothness requirements ensure that the value of χ_k on some element e_k should not differ much from its neighbors χ_j. Define the function

$$\varphi : \bigcup_{k=1}^{N_e}\{e_k\} \to \{1,2,3\}, \quad e_k \mapsto \varphi(e_k) \tag{22}$$

as the number of adjacent triangular elements e_j; call two elements e_p and e_q *adjacent* whenever they share a side. The following stochastic equation reflects the smoothness condition:

$$\chi_k = \frac{1}{\varphi(e_k)}\sum_{i=1}^{\varphi(e_k)}\chi_{k_i} + I_k, \quad I_k \sim \mathcal{N}\big(0,\sigma_k^2\big) \tag{23}$$

for $k = 1, 2, \ldots, N_e$. Element e_{k_i} is a neighbors of e_k and the term I_k is called an innovation term. The innovation term shows that χ_k can vary with respect to its neighbors. The value of σ_k reflects to what extent the value of χ_k can differ with respect to the values of its neighbors. To illustrate this idea, apply (23) to the elements in Fig. 1 to obtain, for example,

$$\begin{aligned}\chi_1 &= \frac{1}{2}(\chi_2 + \chi_4) + I_1\\ \chi_2 &= \frac{1}{3}(\chi_1 + \chi_3 + \chi_5) + I_2.\end{aligned} \tag{24}$$

The set of equations in (23) can be written as

$$R\chi = E \tag{25}$$

where $R \equiv (I_{N_e\times N_e} - S)$ and $E \sim \mathcal{N}(0, \Sigma_{N_e\times N_e})$. The matrix S originates from the right-hand side in (24). Note that the null space of R is 1-D and consists of all uniform χ-distributions. The obtained operator R is used to regularize the solutions. The stochastic model (23) can be used if one defines the minimization problem in terms of a Bayesian framework [2].

In general, if Ω is meshed by means of a nonuniform triangulation, smoothness requirement (23) must be replaced by, for example,

$$\chi_k = \sum_{i=1}^{\varphi(e_k)}\left(\frac{\mu(e_{k_i})}{\sum_{j=1}^{\varphi(e_k)}\mu(e_{k_j})}\right)\chi_{k_i} + I_k, \quad I_k \sim \mathcal{N}\big(0,\sigma_k^2\big) \tag{26}$$

where $\mu(e)$ measures the area of element e. Note that, in the case, the triangulation is uniform, expression (26) reduces to (23).

Tikhonov regularization [2, Ch. 6] means that the original problem is replaced by a nearby minimization problem

$$\chi^* = \underset{\chi\in\mathbb{R}^{N_e}}{\operatorname{argmin}}\, \mathcal{J}(\chi) + \lambda^2\frac{1}{2}\|R(\chi - \chi_{\text{prior}})\|_2^2 \tag{27}$$

where λ is called the regularization parameter. The regularization parameter should be selected in such a way that for the desired solution, the norm of the vector $R(\chi - \chi_{\text{prior}})$ is not excessively large; whenever $\|R(\chi - \chi_{\text{prior}})\|_2$ is small, it follows that χ is relatively smooth. However, it is not

desirable that the norm is close to zero, because it would imply that the found solution merely shows variation.

In general, it is not clear which value for λ is optimal and how to find a suitable value. One heuristic approach is the use of the so-called L-curve [6]. The most favorable value of λ is the one that corresponds to the corner of the L-curve, which gives a good balance between the minimization of the residual and the size of the regularization term. However, the computation of this L-curve is too cumbersome and time-consuming.

F. Inversion, Solving the Minimization Problem

Hereinafter, problem (27) is considered. Note that this problem is not linear in χ. Therefore, the parameter estimation method is based on a nonlinear least-squares problem. A sophisticated (iterative) numerical solver is required to solve this least-squares problem. Recall that a necessary condition for χ^{opt} to be a local minimum for $\mathcal{J}$ is

$$\nabla\left[\mathcal{J}(\chi)+\lambda^2\frac{1}{2}\|R(\chi-\chi_{\text{prior}})\|_2^2\right]\Big|_{\chi=\chi^{\text{opt}}}=\mathbf{0}. \quad (28)$$

In Gauss–Newton-type methods [13, Ch. 3], one requires these gradients with respect to χ for efficient computation of the nonlinear least-squares problem. In general, it is complex to find an analytical expression for this gradient, as the underlying physical model may consist of many nonlinearities. It is favorable to derive analytical expressions for the gradient, as this reduces the computational time significantly. In the Appendix, analytical expressions for the gradient of $\mathcal{J}$ are derived using the adjoint method.

The quasi-Newton method or "BFGS" [13], is used to solve the minimization problem. The BFGS method is a part of the **fminunc** routine in the unconstrained optimization toolbox in `MATLAB` and uses the gradient expressions derived for (27).

In practice, the value of $\mathcal{J}$ is rather small, and therefore, any pre-programed tolerance values are already met, terminating the process. Scaling of the problem avoids this problem. To overcome any numerical problems, we introduce the scaling factor κ in the minimization problem and write

$$\chi^*=\underset{\chi\in\mathbb{R}^{N_e}}{\operatorname{argmin}}\,\kappa\left[\mathcal{J}(\chi)+\lambda^2\frac{1}{2}\|R(\chi-\chi_{\text{prior}})\|_2^2\right]. \quad (29)$$

An appropriate choice for scaling factor κ is

$$\kappa=\left(\mathcal{J}(\chi_0)+\lambda^2\frac{1}{2}\|R(\chi_0-\chi_{\text{prior}})\|_2^2\right)^{-1} \quad (30)$$

for some regularization parameter λ and initial guess χ_0 in the BFGS method.

G. Magnetic Susceptibility Estimation Method

Finally, we propose our main result in this paper. The parameter estimation method, which computes estimations of spatially magnetic susceptibility distributions, is called the "magnetic susceptibility estimation method." We abbreviate our parameter estimation method by **MSEM** and it is defined as follows—based on an initial guess for χ, say χ_0, solve problem (27) for $\lambda = 0$ to obtain a solution of the original problem without any regularization. Then, the obtained solution acts as initial guess for the full problem described in (27), for some nonzero λ. The obtained solution is the estimation for χ. Pseudo-code for this method is found in Fig. 2.

Magnetic Susceptibility Estimation Method:

Input: Set $\chi_0 \in \mathbb{R}^{N_e}, \varepsilon_{tol} \in \mathbb{R}^+, \chi_{prior}$ and $\kappa, \lambda \geq 0$
Output: Minimizer χ^* of problem (27)

1: **function** PARAMETERESTIMATION
2: Use $\mathbf{fminunc}(\chi_0, \varepsilon_{tol})$ to solve

$$\hat{\chi} = \underset{\chi\in\mathbb{R}^{N_e}}{\operatorname{argmin}}\,\mathcal{J}(\chi)$$

3: Use $\mathbf{fminunc}(\hat{\chi}, \varepsilon_{tol})$ to solve

$$\chi^* = \underset{\chi\in\mathbb{R}^{N_e}}{\operatorname{argmin}}\,\mathcal{J}(\chi) + \lambda^2\frac{1}{2}\|R(\chi-\chi_{prior})\|_2^2$$

4: **return** χ^*
5: **end function**

Fig. 2. Magnetic susceptibility estimation method.

It is observed that residual functional (19) is quite insensitive to variations in χ, which makes the search for an optimal solution difficult. This is due to the asymptotic behavior of forward model (12) for $\chi \to \infty$. Rescaling the problem via (29) and (30) allows the BFGS method to find a local optimal solution. This solution is then used in the **MSEM** to find a more optimal regularized solution.

III. NUMERICAL EXAMPLES

In this section, two numerical examples are given. First, the integral equation is solved for a square plate to obtain the induced magnetization $\mathbf{M}$, and then the corresponding reduced magnetic field is computed in a plane above the plate. The typical shape of the solution $\mathbf{M}$ shows that the integral equation is implemented correctly. Then, an identical-twin experiment is conducted to test the methodology.

A. Solving the Integral Equation

Consider the following simple example: a square plate Ω that is 1 m long and 10 mm thick is placed in a uniform external magnetic field given by

$$\mathbf{B}_0 = [60, 0, 0]^T \quad (\mu T). \quad (31)$$

Suppose that the magnetic susceptibility is uniform on Ω and $\chi \equiv 100$; the plate is meshed into 50 triangular elements. The condition number of system (12) is approximately 28, which means that the system is well conditioned. Therefore, the problem may be solved using an LU or SVD decomposition. If we compactly write system (12) as $K\mathbf{M} = \mathbf{b}$, then matrix K can be decomposed using an LU decomposition: $K = LU$, where L is a $3M \times 3M$ lower triangular matrix with the value one on the diagonal entries, and U is a $3M \times 3N$ matrix with zero entries below the main diagonal. In the case of an SVD decomposition, we can write $K = SUV^T$, where S and V are orthogonal matrices and U contains the singular values

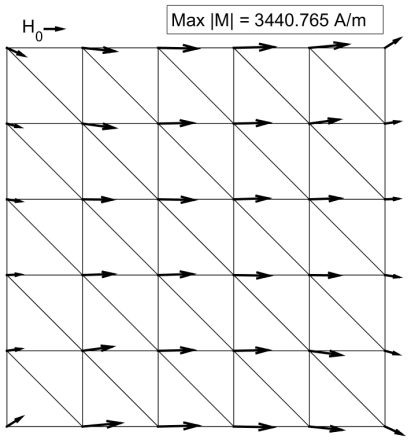

Fig. 3. Induced magnetization on a square plate for $\chi \equiv 100$, placed in a uniform background field $\mathbf{H}_0 = 50\mathbf{u}_x$ A/m.

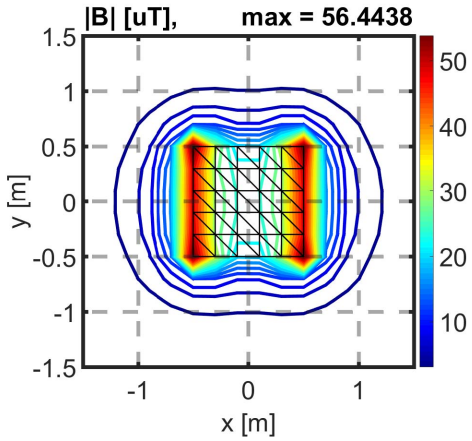

Fig. 4. Reduced magnetic induction field 5 cm above the plate.

of K. Using these decompositions, one can solve system (12) easily (see [13]). The resulting magnetization distribution $\mathbf{M}$ is shown in Fig. 3. Note that the induced magnetization is more or less parallel to the background field, as expected. At 5 cm above Ω, the corresponding magnetic field is computed. The results are shown in Fig. 4.

B. Twin Experiment for Parameter Estimation

Identical-twin experiments [1] use a model to generate a set of "observations," add random noise to the simulated observations, and then try to estimate the true model parameters, using these noisy observations and the **same** model. This type of experiment is a natural first step, because it limits the sources of errors to a minimum and it enables us to understand whether or not the estimation method acts consistently to simulated data.

Our estimation method is tested on a square steel plate using an identical-twin experiment. Start with a plate with a length L of 1 m, a width W of 1 m, and 10 mm thickness. Suppose a continuous χ distribution is given by

$$\chi(\mathbf{r}) = 70 + 30\cos(2\|\mathbf{r} + \mathbf{c}\|_2), \quad \mathbf{c} = \frac{1}{2}[L, L]^T. \tag{32}$$

The vector $\mathbf{c}$ indicates the center of the plate. The above-mentioned definition of χ defines a smooth varying χ-pattern of the plate. The plate is meshed into $N_e = 200$ triangular elements. In each element, we compute the value χ using (32). This leads to the true model parameters $\chi_{\text{true}} \in \mathbb{R}^{200}$, as depicted in Fig. 5(a).

For the above-mentioned plate with magnetic susceptibility χ_{true}, generate a set of $M = 225$ measurements of the reduced near field in a uniform sampling grid $(1/2)[-L, L]^2$ at $z = 1$ cm above the plate and form $\mathbf{B}_c^m \in \mathbb{R}^{3M}$ using (12), (13), and (15). Gaussian white noise is added to each component of $\mathbf{B}_c^m$

$$\mathbf{B}^m = \mathbf{B}_c^m + \mathbf{e}, \quad \mathbf{e} \sim \mathcal{N}\big(0, \sigma^2 I_{3M\times 3M}\big). \tag{33}$$

We choose $\sigma = 10^{-6}$ in the above-mentioned error vector, which means that there is approximately $3\mu T$ variation in each component. In practice, magnetic sensors have a measurement error in the order of $1nT$, but in this twin experiment, we want to push the boundaries of the performance of **MSEM**. Set

$$\chi_0 \equiv 70, \quad \chi_{\text{prior}} \equiv 0, \ \lambda = 10^{-11} \tag{34}$$

and apply the **MSEM** to the above set of noisy measurements. The results of $\hat{\chi}$ and χ^* are depicted in Fig. 5(b) and (c). Note the influence of regularization on the obtained estimate χ^*. Regularization not only steers the iterative solver to a better minimizer, but we are even able to reconstruct the true χ-pattern with a high accuracy. In Figs. 6 and 7, the iterative process in the second step of **MSEM** is shown. Note that, for a nonlinear problem, the convergence of the problem is sufficiently fast.

In Fig. 5(d) and (e), the difference and relative error between χ_{true} and χ^* are depicted; the relative error is pointwise defined by

$$\tau = \frac{|\chi^* - \chi_{\text{true}}|}{|\chi_{\text{true}}|}. \tag{35}$$

A maximum relative error 0.05 is quite acceptable. Based on these results, we conclude that the twin experiment is successful.

C. Experiment Design

Based on the numerical identical-twin experiment, a real experiment for the characterization of the magnetic materials can be designed as follows. The performance of the estimation method is dependent on the chosen measurement configuration. The twin experiment could be used to determine the optimal sensor configuration. Start with defining a true magnetic susceptibility pattern χ_{true}. If no *a priori* knowledge about the material is known (such as anomalies in the material), the pattern χ_{true} should be chosen uniformly. For given sensor configuration S, let χ_S denote the corresponding solution of the **MSEM**. To find an optimal sensor configuration, we could solve the following minimization problem:

$$S^* = \arg\min_{S\in\mathcal{S}} V_N(S) \tag{36}$$

where N is the size of the susceptibility pattern (dependent on the chosen mesh), $\mathcal{S}$ is the set of all possible sensor

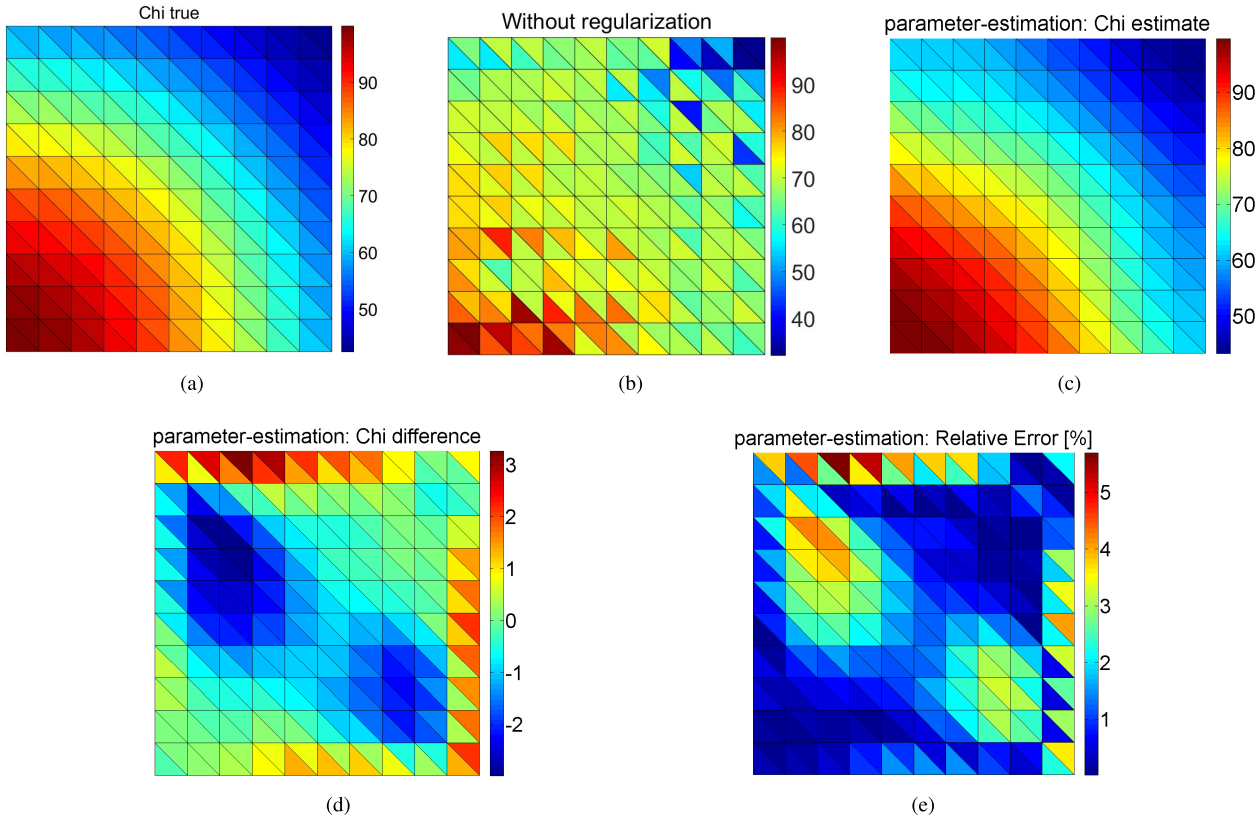

Fig. 5. Twin-experiment results for MSEM. Spatial distributions (a) χ_{true}, (b) $\hat{\chi}$ (without regularization), (c) χ^* (with regularization), (d) absolute error $\chi^* - \chi_{\text{true}}$, and (e) relative error $(\chi^* - \chi_{\text{true}})/\chi_{\text{true}}$.

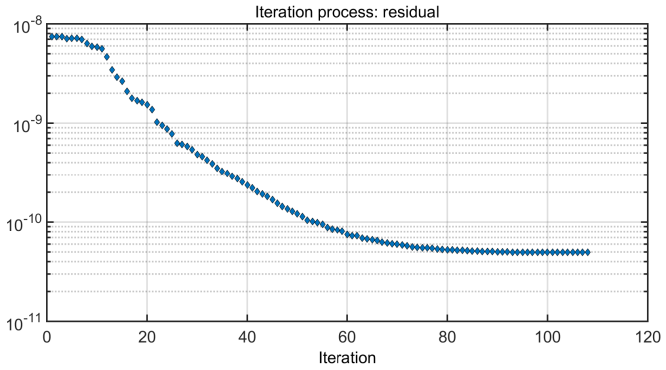

Fig. 6. Values of the residual function during the iterative process.

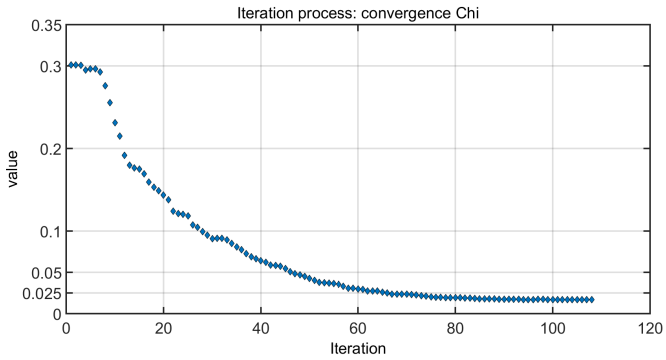

Fig. 7. Relative error in χ during the iterative process.

configurations, and

$$V_N(S) = \sum_{i=1}^{N} (\chi_S(i) - \chi_{\text{true}}(i))^2 \tag{37}$$

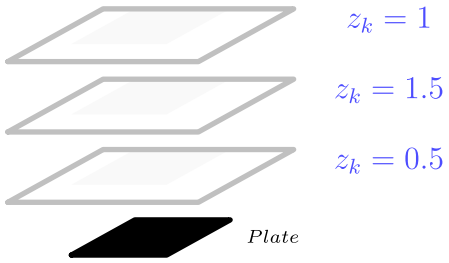

Fig. 8. Measurements planes above plate for several values of z.

is the empirical variance in the susceptibility pattern. Note that the solution depends on the chosen true pattern χ_{true}.

Furthermore, as a rule of thumb, the measurements should take place near the magnetic object, and in such a way that the shape of the induced magnetic field is represented in the data set. If the measurements take place too far away from the magnetic object, then the method is not able to determine the local variations of the χ-pattern inside the magnetic object. If an optimal sensor configuration is found using this routine, a real experiment can be defined to determine the magnetic susceptibility of a real magnetic object.

Finally, note that we have assumed that there is no permanent magnetization present in the magnetic object. In practice, there is a permanent component present. Therefore, any data set of measurements of the magnetic field is spoiled by this component. One should filter out this contribution in the data set first, before it can be used in the **MSEM** method. This is easily done by considering two measurements of the magnetic object in different background fields. By a suitable subtraction,

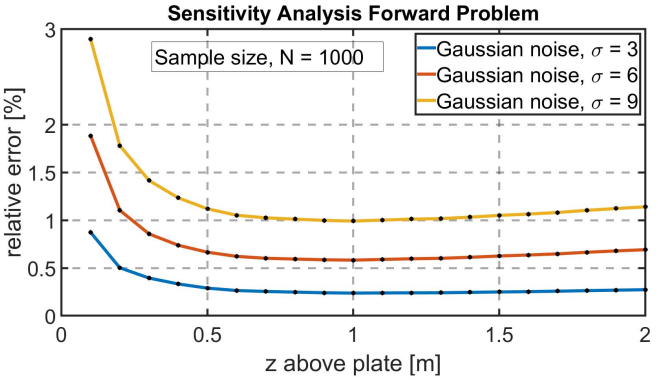

Fig. 9. Monte Carlo simulation results for system (12). The maximum mean relative error between the true magnetic field and the computed fields.

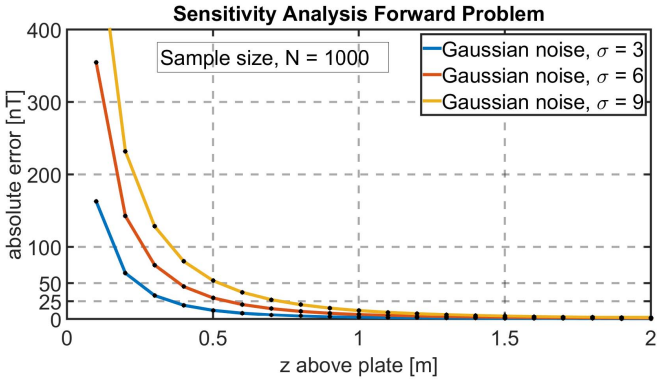

Fig. 10. Monte Carlo simulation results for system (12). The maximum mean absolute error between the true magnetic field and the computed fields.

one is left with a data set that is related to the linear behavior and can be used for the estimation method.

IV. Sensitivity Analysis

In the identification of magnetic states of objects, it is evident that an accurate estimation of χ is required. By means of the MEMS method, we can estimate the true χ-distribution in some magnetic object. However, small differences between the estimation and the true distribution will remain, and it is important to understand how this difference propagates in the reduced magnetic field at larger distances. The purpose of this section is to understand the statistical properties of the forward model described in (11).

A. Forward Propagation of Magnetic Susceptibility

We investigate the statistical properties of the forward problem, by means of a Monte Carlo simulation. As before, consider a square plate with sides of 1 m and a thickness of 10 mm. Discretize the square plate into 200 triangular elements and assume that the magnetic susceptibility is 100 on each triangular element; denote this magnetic susceptibility distribution by χ_0. Define a realization of the magnetic susceptibility in the Monte Carlo simulation by

$$\chi_k = \chi_0 + (\Delta\chi)_k, \quad (\Delta\chi)_k \sim \mathcal{N}(0, \sigma^2) \tag{38}$$

for each $k = 1, 2, \ldots, N$, where N denotes the sample size in the Monte Carlo simulation. In our Monte Carlo simulation, we set $N = 1000$. For χ_0 and each realization χ_k, we compute the reduced magnetic induction field in several planes above the plate (see Fig. 8).

In each plane, we compare the magnetic induction field corresponding to χ_0, denoted by $\mathbf{B}_0^z$, with the magnetic induction fields $\mathbf{B}_k^z$ of the realizations at height z. These comparisons give rise to the relative error and the maximum error at height z defined by

$$\tau_k^z = \frac{\left\|\mathbf{B}_0^z - \mathbf{B}_k^z\right\|_2}{\left\|\mathbf{B}_0^z\right\|_2} \tag{39}$$

and

$$\varepsilon_k^z = \left\|\mathbf{B}_0^z - \mathbf{B}_k^z\right\|_2 \tag{40}$$

for each realization $k = 1, 2, \ldots, N$. The mean values

$$\tau^z = \frac{1}{N}\sum_{k=1}^{N} \tau_k^z \quad \text{and} \quad \varepsilon^z = \frac{1}{N}\sum_{k=1}^{N} \varepsilon_k^z \tag{41}$$

are shown in Figs. 9 and 10, for several values of σ. In this analysis, we considered the values $\sigma = 3, 6, 9$. Using a rule of thumb for Gaussian distributions this implies that the variations $(\Delta\chi)_k$ fall within the interval $[-3\sigma, 3\sigma]$ with a probability of 0.99. This means that we consider variations in each component in the order of 10, 20, and 30 nanotesla, respectively.

Note that the absolute error vanishes for increasing z, as expected. For $z \geq 1$ m, the variations $(\Delta\chi)_k$ are not visible anymore. However, if we look at the relative errors, the relative error becomes constant[3] for larger z. This is also as expected, as the magnetic intensity of the field decreases as $(1/r^3)$, where r is the distance from the source.

V. Conclusion

In this paper, we proposed a method to estimate the magnetic susceptibility of a magnetic object. This method can be applied to any (ferro)-magnetic material, under the assumption that the object itself has a sufficiently small thickness compared to the other dimensions of the object. The estimation method is based on a nonlinear least-squares optimization problem and is solved via the BFGS method. Based on an identical-twin experiment, we have seen that the method shows a very good fit; under reasonable large measurement errors, the **MSEM** method is still able to estimate an accurate distribution of the magnetic susceptibility. An interesting next step is to see how the parameter method performs in practice.

Moreover, a sensitivity analysis has shown that it is not strictly necessary to estimate the magnetic susceptibility distribution with a high accuracy, if we want to use these distributions in accurate descriptions of the reduced magnetic field. Small variations in the magnetic susceptibility distribution are only locally observable in the induced magnetic field. Based on an error analysis, the local variations in the magnetic

[3]Indeed, the values for the relative errors at $z = 2$ are slightly higher, but this is probably due to numerical errors in the computations.

susceptibility in a square plate are not visible in the induced magnetic field at a distance approximately the size of the plate.

Future work is to test and validate the **MSEM** method on a real magnetic plate. Using experimental data, it should become clear to what extent the method is able to estimate the magnetic susceptibility distribution accurately. However, this is not an easy task as the true magnetic susceptibility distribution is unknown in practice. Therefore, validation of the results will be complicated. An experimental design can be developed to determine which measurements are necessary to obtain the magnetic susceptibility of magnetic materials.

APPENDIX
ADJOINT METHOD FOR GRADIENT COMPUTATIONS

In this appendix, the gradient of the object functionals (19) and (27) are computed, by means of the adjoint method [5], [20]. Note that the underlying physical model can be written as

$$F(\mathbf{M}, \chi) = \mathbf{0} \tag{42}$$

where F reads

$$F(\mathbf{M}, \chi) := \left[\sum_{k=1}^{N_e} \frac{1}{\chi_k} D_k + A + B\right] \mathbf{M} - \mathbf{h}_0. \tag{43}$$

The idea behind the adjoint method is to consider the object functional

$$\mathcal{J}(\chi) = \frac{1}{2} \mathbf{Res}^T W \mathbf{Res} - L^T F(\mathbf{M}, \chi) \tag{44}$$

which is equivalent to (19) and where L is called the adjoint variable. Note that L acts as a Lagrange multiplier. The two object functions are equivalent for each choice of L, due to (42). Variation of $\mathcal{J}$ with respect to variable χ_j is given by

$$\begin{aligned} \Delta \mathcal{J}_j &= \mathbf{Res}^T W \frac{\partial \mathbf{Res}}{\partial \mathbf{M}} \Delta \mathbf{M} - L^T \left(\frac{\partial F}{\partial \mathbf{M}} \Delta \mathbf{M} + \frac{\partial F}{\partial \chi_j} \Delta \chi_j \right) \\ &= -L^T \frac{\partial F}{\partial \chi_j} \Delta \chi_j + \left(g^T - L^T \frac{\partial F}{\partial \mathbf{M}} \right) \Delta \mathbf{M} \end{aligned} \tag{45}$$

where g^T is given by

$$g^T := \mathbf{Res}^T W \frac{\partial \mathbf{Res}}{\partial \mathbf{M}}. \tag{46}$$

Choose the adjoint variable L by solving the equation

$$\left(\frac{\partial F}{\partial \mathbf{M}} \right)^T L = g \tag{47}$$

such that the last term in (45) vanishes. For this choice of L, the jth component of the gradient of (19) reads

$$(\nabla \mathcal{J})_j = -L^T \frac{\partial F}{\partial \chi_j}. \tag{48}$$

It remains to derive analytical expressions for the partial derivates in (45). Some fruitful computations yields

$$\frac{\partial F}{\partial \mathbf{M}} = \sum_{k=1}^{N_e} \frac{1}{\chi_k} D_k + A + B, \quad \frac{\partial F}{\partial \chi_j} = -\frac{1}{\chi_k^2} D_k \mathbf{M}. \tag{49}$$

The partial derivative $(\partial \mathbf{Res}/\partial \mathbf{M})$ is in general difficult to compute, but (17) yields that

$$\frac{\partial \mathbf{Res}}{\partial \mathbf{M}} = C(\mathcal{M}). \tag{50}$$

Next, the gradient of (27) is computed. Using the previous computations, only the gradient of the second term in this expression remains. A simple computation shows that

$$\nabla \left[\frac{1}{2} (\chi - \chi_0)^T R^T R (\chi - \chi_0) \right] = R^T R (\chi - \chi_0) \tag{51}$$

because $R^T R$ is symmetric. Combining results (48) and (51) yield the gradient of (27).

ACKNOWLEDGMENT

This work was supported by the Dutch Ministry of Defence.

REFERENCES

[1] L. Bengtsson, M. Ghil, E. Källen, Eds., *Dynamic Meteorology: Data Assimilation Methods*. New York, NY, USA: Springer, 1981, p. 330.
[2] D. Calvetti and E. Somersalo, *An Introduction to Bayesian Scientific Computing*. New York, NY, USA: Springer-Verlag, 2007.
[3] O. Chadebec, J.-L. Coulomb, J.-P. Bongiraud, G. Cauffet, and P. Le Thiec, "Recent improvements for solving inverse magnetostatic problem applied to thin hulls," *IEEE Trans. Magn.*, vol. 38, no. 2, pp. 1005–1008, Mar. 2002.
[4] O. Chadebec, J. L. Coulomb, G. Cauffet, and J. P. Bongiraud, "How to well pose a magnetization identification problem," *IEEE Trans. Magn.*, vol. 39, no. 3, pp. 1634–1637, May 2003.
[5] M. B. Giles and N. A. Pierce, "An introduction to the adjoint approach to design," *Flow, Turbulence Combustion*, vol. 65, nos. 3–4, pp. 393–415, Dec. 2000.
[6] P. C. Hansen and D. P. O'leary, "The use of the L-curve in the regularization of discrete Ill-posed problems," *SIAM J. Sci. Comput.*, vol. 14, no. 6, pp. 1487–1503, Jul. 1993.
[7] J. J. Holmes, *Exploitation of A Ship's Magnetic Field Signatures*. San Rafael, CA, USA: Morgan & Claypool, 2006.
[8] J. J. Holmes, *Modeling a Ship's Ferromagnetic Signatures*. San Rafael, CA, USA: Morgan & Claypool, 2007.
[9] J. J. Holmes, *Reduction of a Ship's Magnetic Field Signatures*. San Rafael, CA, USA: Morgan & Claypool, 2008.
[10] J. D. Jackson, *Classical Electrodynamics*, 3rd ed. New York, NY, USA: Wiley, 1999.
[11] D. C. Jiles and D. L. Atherton, "Theory of ferromagnetic hysteresis," *J. Magn. Magn. Mater.*, vol. 61, nos. 1–2, pp. 48–60, Sep. 1986.
[12] B. Kressler, L. D. Rochefort, T. Liu, P. Spincemaille, Q. Jiang, and Y. Wang, "Nonlinear regularization for per voxel estimation of magnetic susceptibility distributions from MRI field maps," *IEEE Trans. Med. Imag.*, vol. 29, no. 2, pp. 273–281, Feb. 2010.
[13] J. Nocedal and S. Wright, *Numerical Optimization*. New York, NY, USA: Springer Text, 1999.
[14] J. A. Osborn, "Demagnetizing factors of the general ellipsoid," *Phys. Rev. J. Arch.*, vol. 67, nos. 11–12, p. 351, Jun. 1945.
[15] N. G. Sepúlveda, I. M. Thomas, and J. P. Wikswo, Jr., "Magnetic susceptibility tomography for three-dimensional imaging of diamagnetic and paramagnetic objects," *IEEE Trans. Magn.*, vol. 30, no. 6, pp. 5062–5069, Nov. 1994.
[16] O. J. G. Somsen and G. P. M. Wagemakers, "Separating permanent and induced magnetic signature: A simple approach," *Int. J. Electron. Commun. Eng.*, vol. 9, no. 10, pp. 1236–1239, Mar. 2015.
[17] L. Sun, X. Liu, D. Jia, and H. Niu, "Three-dimensional stress-induced magnetic anisotropic constitutive model for ferromagnetic material in low intensity magnetic field," *AIP Adv.*, vol. 6, no. 9, p. 095226, Sep. 2016.
[18] E. D. Torre, *Magnetic Hysteresis*. Hoboken, NJ, USA: Wiley, 1999.
[19] Y. Vuillermet *et al.*, "Scalar potential formulation and inverse problem applied to thin magnetic sheets," *IEEE Trans. Magn.*, vol. 44, no. 6, pp. 1054–1057, Jun. 2008.
[20] M. A. Zaman, P. C. Hansen, L. T. Neustock, P. Padhy, and L. Hesselink, "Adjoint method for estimating Jiles-Atherton hysteresis model parameters," *J. Appl. Phys.*, vol. 120, no. 9, p. 093903, Aug. 2016.